

Nanoscale

Accepted Manuscript



This is an *Accepted Manuscript*, which has been through the Royal Society of Chemistry peer review process and has been accepted for publication.

Accepted Manuscripts are published online shortly after acceptance, before technical editing, formatting and proof reading. Using this free service, authors can make their results available to the community, in citable form, before we publish the edited article. We will replace this *Accepted Manuscript* with the edited and formatted *Advance Article* as soon as it is available.

You can find more information about *Accepted Manuscripts* in the [Information for Authors](#).

Please note that technical editing may introduce minor changes to the text and/or graphics, which may alter content. The journal's standard [Terms & Conditions](#) and the [Ethical guidelines](#) still apply. In no event shall the Royal Society of Chemistry be held responsible for any errors or omissions in this *Accepted Manuscript* or any consequences arising from the use of any information it contains.



Nanoscale

COMMUNICATION

Enzymatically Degradable Hybrid Organic-Inorganic Bridged Silsesquioxane Nanoparticles for In-Vitro Imaging

Received 00th January 20xx,
Accepted 00th January 20xx

Y. Fatieiev,^a J. G. Croissant,^a K. Julfakyan,^a L. Deng,^a D. H. Anjum^b, A. Gurinov^b and N. M. Khashab^{a*}

DOI: 10.1039/x0xx00000x

www.rsc.org/

We describe biodegradable bridged silsesquioxane (BS) composites nanomaterials with unusually high organic content (ca. 50%) based on oxamide components mimicking amino-acid bioleavable groups. Unlike most bulk BS materials, the design of sub-200 nm nearly monodisperse nanoparticles (NPs) was achieved. This study is the first example for enzymatically-degradable BS NPs, however, promising imaging nanoprobles.

Nanomedicine has emerged as an extensive subject of investigation and applications around the world due to the discovery of the unique diagnostic and therapeutic advantages of nanomaterials.¹⁻¹⁴ The nanoscale dimension of such materials endows them with long blood circulation times as well as preferential accumulation in cancerous tissues with the so-called enhanced permeation and retention effect.^{15, 16} However, one of the crucial challenges to be addressed for their future applications is the ability to degrade in biological environment. Biodegradability of nanomaterials is indeed expected to be the safest route to avoid largely-unknown and potentially harmful side-effects of accumulated nanoparticles (NPs) in the human body. Thus, the cytotoxicity of both nanomaterials and their degradation products should be very low, and NPs should be degraded shortly after the fulfillment of their biomedical purpose.¹⁷

Biodegradable NPs could be divided into three groups: polymeric, inorganic and organic-inorganic hybrid nanomaterials. Among polymeric particles, polylactic acid (PLA),¹⁸ polylactide-co-glycolide (PLGA)¹⁹ and poly(β -amino ester) (PBAE)¹⁷ are the most utilized.²⁰ Calcium phosphate,²¹ manganous phosphate,²² and porous silicon²³ are examples of biodegradable inorganic NPs. Additionally, biodegradable organic-inorganic hybrid NPs such as periodic mesoporous organosilica have been reported.²⁴ The hybrid nature of organosilica was designed to increase the biodegradability of silica²⁵ with a high content of organic functionalities in the matrix for

biomedical applications. Effective biodegradation could be achieved by the homogeneous distribution of cleavable functional groups²⁶ via different stimuli such as redox reactions,²⁴ pH change,²⁷ and light actuation.²⁸

Among organic-inorganic hybrid nanomaterials bridged silsesquioxane (BS) nanoplatforms have been recently described for few biomedical applications.²⁹⁻³⁴ Indeed, such materials of general formula $O_{1.5}Si-R-SiO_{1.5}$ are constituted of high contents of organic R bridging groups (~40-60 wt%) in a robust and easily functionalized silica matrix.³⁵ Thus, the properties of BS NPs could be widely tuned according to the organic groups presenting in the bridged organoalkoxysilane sol-gel precursors.³⁵ It is noteworthy that the synthesis of BS NPs for biomedical application is challenging since the absence of silica source (e.g. tetraethoxysilane) during the condensation of bridged-organoalkoxysilanes generally leads to bulk, micro-sized particles, or aggregated NPs. In this context, Shea *et al.* reported BS NPs with light-triggered charge reversal features for anti-body release.³³ Lin *et al.* reported BS NPs composed of oxaliplatin bridges for cancer therapy.^{34, 36} Croissant and coworkers prepared two-photon-sensitive BS NPs for efficient photodynamic therapy and bioimaging applications.²⁹ Wong Chi Man *et al.* reported pH-sensitive BS NPs for the release of cyanuric acid attached via hydrogen bonds with the BS matrix as a model of drug delivery system in lysosomal acidity.³⁰ Ester-bridged silsesquioxane-coated liposomes were applied for drug delivery.³⁷ Only one study has been reported on biodegradable BS NPs which consisted of gadolinium-complexed bridges with disulfide linkages which can be cleaved by glutathione for MRI imaging.³⁸ However, among the variety of stimuli-degradable groups, carbamate, ester and amide linkers should be additionally distinguished as enzymatically degradable and were not previously described in BS NPs.²⁶

Herein we report the controlled synthesis of biodegradable sub-200 nm non-aggregated dense BS NPs via sol-gel reaction of an oxamide-bridged alkoxy silane (OBA) precursor inspired from the nature with the common enzymatically-catalyzed metabolism processes (see Figure 1). Moreover, fluorescent BS NPs were obtained via incorporation of fluorescein isothiocyanate moieties inside the siloxane framework. Both materials were fully characterized via various techniques displaying the high organic content and functionalities of the NPs. Additionally, the

^a Smart Hybrid Materials Laboratory, Advanced Membranes and Porous Materials Center, King Abdullah University of Science and Technology, Thuwal 23955-6900, Kingdom of Saudi Arabia. E-mail: niveen.khashab@kaust.edu.sa.

^b Advanced Nanofabrication, Imaging and Characterization Laboratory, King Abdullah University of Science and Technology, Thuwal 23955-6900, Saudi Arabia.

† Electronic supplementary information (ESI) available: Detailed synthetic procedure, experimental procedure and Fig. S1–15 See DOI: 10.1039/x0xx00000x

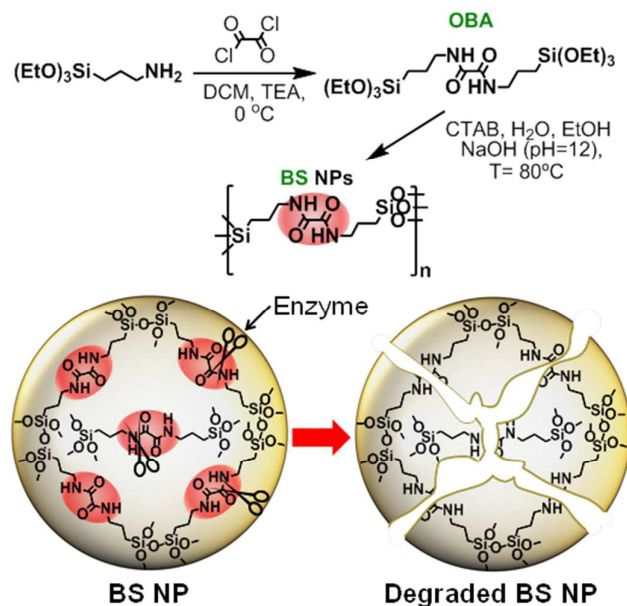


Fig. 1. Schematic representation of the synthesis and enzymatic degradation of BS NPs via the cleavage of amide bonds.

enzymatically mediated degradation of NPs in simulated biological media was demonstrated, and fluorescent BS nanoprobe were applied for in-vitro imaging in cancer cells.

The OBA precursor was synthesized by coupling of oxalyl chloride with 2 equivalent of 3-aminopropyltriethoxysilane in dichloromethane using triethylamine as a base catalyst at 0°C (ESI, Figure S1). Nuclear magnetic resonance (NMR), Fourier transform infrared (FTIR) and mass spectroscopies confirmed the completion of the reaction of the OBA (*N,N'*-bis(3-(triethoxysilyl)propyl)oxamide) precursor (ESI, Figures S2-3). BS nanomaterials were then prepared by the addition of an ethanolic solution of OBA to an aqueous basic solution (pH 12) containing the cetyltrimethylammonium bromide (CTAB) surfactant (see Figure 1). Besides, positively-charged oxamide-fluorescein fluorescent BS NPs (BS-FITC) were obtained in similar conditions via the co-condensation of OBA, fluorescein isothiocyanate-alkoxysilane and aminopropyltriethoxysilane.

The nanomaterials physico-chemical characteristics were then characterized by various techniques. Scanning and transmission electron microscopies (SEM, TEM, see Figure 2A-D) displayed nearly monodisperse spherical BS and BS-FITC NPs with average sizes of 125 and 92 nm respectively (Figure 2E-F). In regard to composition, the successful incorporation of organic moieties within the siloxane framework was investigated by scanning transmission electron microscopy (STEM) combined with electron energy-loss spectroscopy (EELS, see a typical spectrum in Figure S4). The uniform distribution of oxamide groups within BS-FITC and BS NPs was demonstrated by STEM-EELS elemental mappings of silicon, oxygen, nitrogen and carbon atoms (Figures 3A and S5 respectively). Moreover, such analysis also proved the homogeneous distribution of the sulfur-containing FITC dyes (Figure 3A), with a clear signal of sulfur in BS-FITC NPs when compared to BS NPs (Figure 3B). Such an observation is often a requirement in dye-

doped nanomaterials in order to maintain intense fluorescence properties. The preservation of oxamide groups was confirmed by the presence of the $\nu_{\text{C}=\text{O}}$ stretching mode of the amide-I at 1668 cm^{-1} in the OBA precursor and 1669 cm^{-1} in BS NPs and BS-FITC NPs (Figure S6). Besides, with red-shift of the $\nu_{\text{Si}-\text{O}}$ mode from 1080 cm^{-1} in OBA precursor to $1090\text{--}1140\text{ cm}^{-1}$ in the BS and BS-FITC NPs indicates the high condensation of the siloxanes. Such conclusions are further confirmed by solid state NMR of ^{13}C and ^{29}Si nuclei, displaying the environments of the oxamide as well as the major proportion of T^2 and T^3 silicon environments for BS and BS-FITC NPs (Figures S7-S8). Thermo-gravimetric analyses depicted weight loss of ca. 50% between 400 and 700°C associated with the decomposition of the high content of organic bridges (Figures S9-10).^{39, 40}

The texture and structure of BS NPs were further assessed by nitrogen sorption analysis. The CTAB surfactant, which was found necessary to obtain non-aggregated nanospheres, was partially extracted in the resulting NPs as shown by FTIR and ^{13}C NMR analyses (Figures S11 and S7). The remaining residues were entrapped in the materials.^{41, 42} Dried BS and BS-FITC NPs were non-porous via porosimetry measurements with surface areas under $25\text{ m}^2/\text{g}$ (data not shown) which is typical of self-assembled BS.⁴³⁻⁴⁵

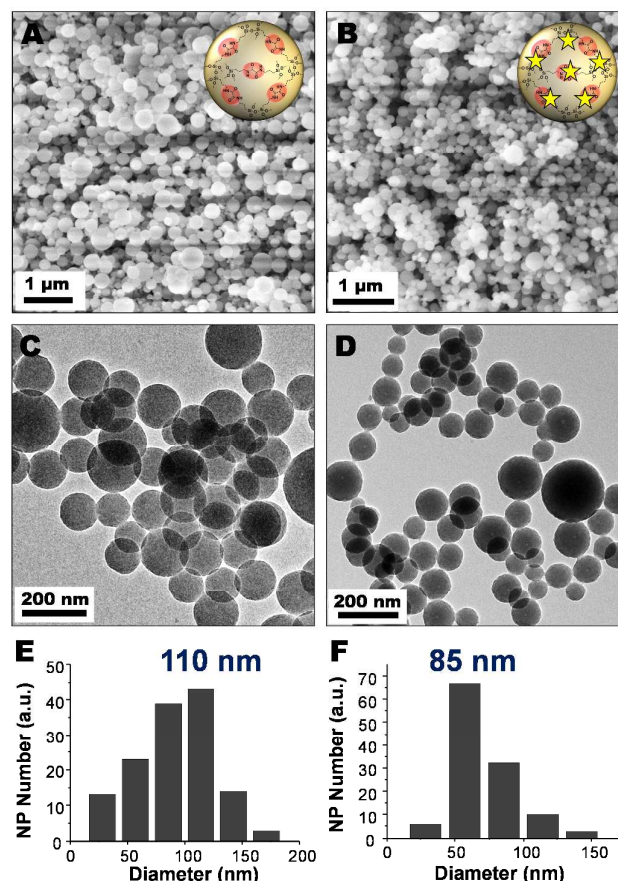


Fig. 2. SEM (A-B) and TEM (C-D) images of BS and BS-FITC NPs. TEM statistical size distributions of BS (E) and BS-FITC NPs (F).

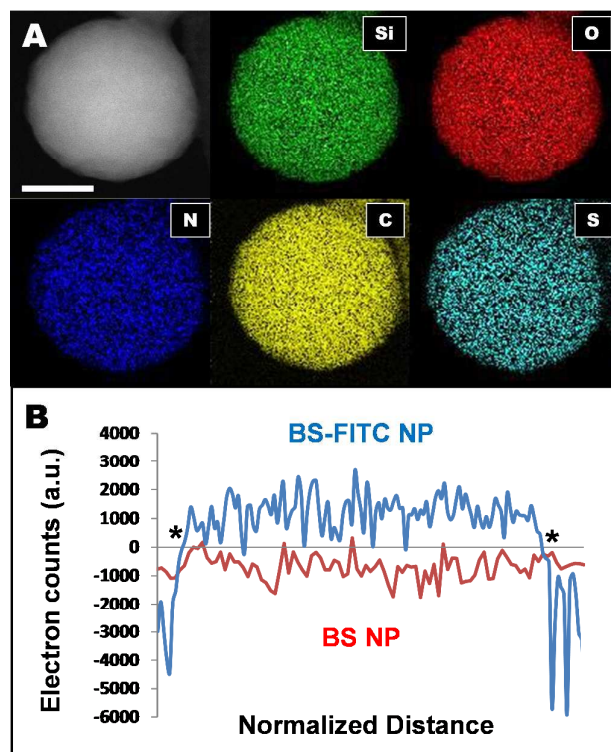


Fig. 3. STEM-EELS elemental mapping (silicon, oxygen, nitrogen, carbon, sulfur) of a representative BS-FITC NP (A). Scale bar of 50 nm. Comparison of the sulfur signal in the BS-FITC and BS NPs demonstrating the homogeneous FITC dye incorporation in BS-FITC NPs (B). *Asterisks encompass the diameter of NP.

Accordingly, the incorporation of organic bridges into the silica framework lead to the formation of parallel nanosized channels as shown by high-resolution TEM (HRTEM, see Figure S12). This is most-likely resulting from intermolecular hydrogen bonds between oxamide groups, as reported with macroscaled BS materials.⁴⁶⁻⁴⁸

The biodegradability of BS NPs was then investigated in simulated biological media. Nanomaterial suspensions in Tris buffer (pH=4), PBS buffer (pH=7.4), and trypsin enzyme in PBS (pH=7.4) buffer were stirred at 37°C during 24 and 48 h. Experimental results showed that BS NPs were only degraded in the presence of trypsin enzymes. This conclusion was supported by TEM images before and after enzymatic degradation (Figure 4A-B), as well as dynamic light scattering (DLS) measurements after 24 and 48 h which depicted the expected decrease of the NPs size (Figure 4C). The initial average hydrodynamic diameter of 295 nm turned into 122 nm after 48 h stirring with trypsin-PBS. The trypsin enzyme is known to cleave amino-acids into carboxylate and ammonium groups,⁴⁹ which is the most likely mechanism in the degradation as suggested by the decrease of oxamide vibration modes in the FTIR spectrum of degraded NPs (see Figure S13). The same results were observed in BS-FITC nanomaterials (Figure S14).

Fluorescent BS-FITC NPs were then applied as nanoprobe in cancer cells. Indeed, BS-FITC NPs have the yellow fluorescence of fluorescein which absorbs light at 505 nm (see Figure S15) and could thus be envisioned for biomedical diagnosis. BS-FITC NPs were also designed to be positively-charged with aminopropyl groups on their

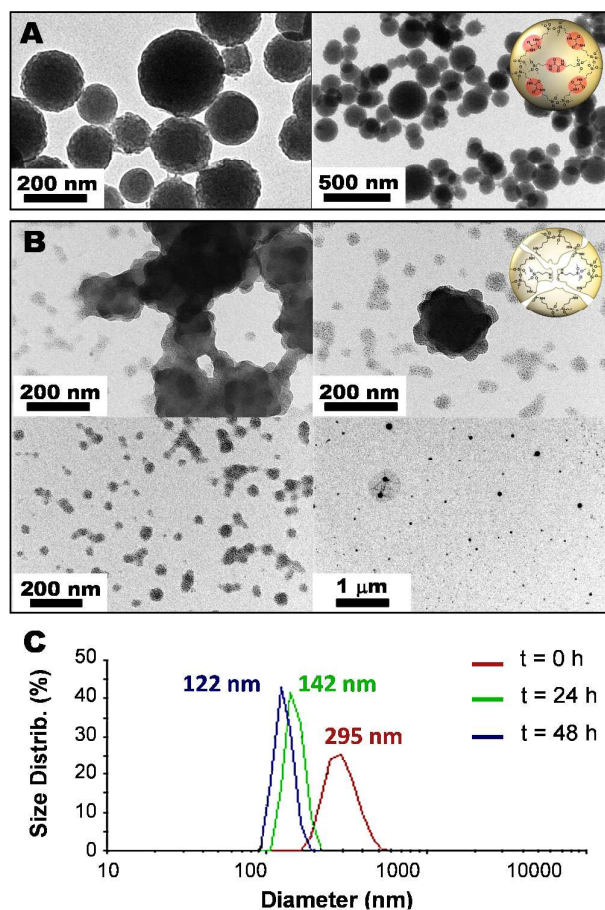


Fig. 4. TEM images of BS NPs in PBS buffer (A), and in trypsin-PBS buffer (B) after 24 h. DLS analyses of the as prepared BS NPs before and after 24 and 48 h of enzymatic degradation.

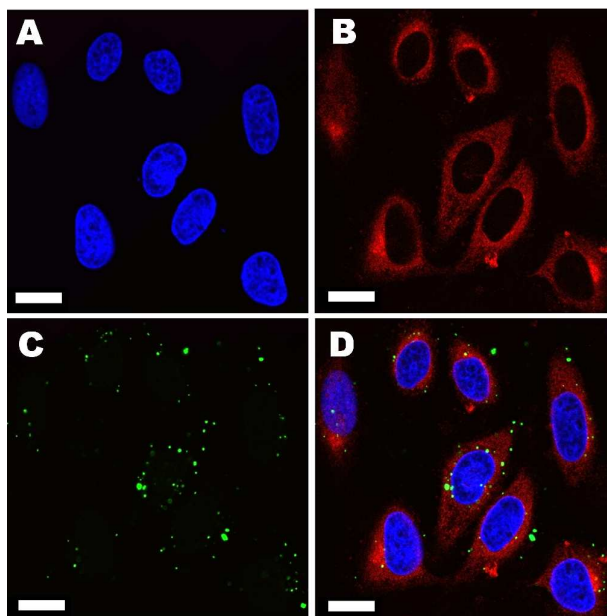


Fig. 5. CLSM images of BS-FITC NPs. Nuclei are stained in blue with DAPI dyes (A), cells membranes in red with CellMask™ (B), and BS-FITC appear with the green fluorescence (C, merged in D). Scale bars of 20 μ m.

surface in order to increase the cellular uptake as reported in the literature.^{50,51} While BS NPs were negatively-charged (-38 mV) due to silanolate groups, the zeta potential of BS-FITC NPs was thus increased to +45 mV (Figure S16). The HeLa cell line was selected, and the biocompatibility of BS NPs was first demonstrated with a complete cell survival up to 100 µg/mL (Figure S17). Secondly, fluorescent NPs were incubated and tracked in cancer cells. Nuclei were stained in blue with DAPI dyes (Figure 5A), and cell membrane in red with CellMask™ (Figure 5B). After only 6 h of incubation, a significant population of the NPs was endocytosed (see Figures 5C-D and S18-19) as witnessed by the intense green fluorescence of the designed nanoprobe within cells (Figure 5D).

Conclusions

In summary, we describe for the first time enzymatically-degradable bridged silsesquioxane hybrid nanomaterials based on nature-inspired oxamide bridges with the organosilica framework. The designed nanomaterials were non-aggregated with biologically relevant sizes for preferential accumulation in tumors. The unique constitution of the materials with a very high organic content (~50%) was found to be homogeneously distributed within individual particle which is probably key for the degradation behavior of the system. The biodegradation of NPs was demonstrated in the presence of the trypsin enzymes in simulated biological media. Furthermore, such nanoplateform could be rendered fluorescent via fluorescein dyes in order to image cancer cells. We are currently studying the impact of the porosity on the extent and kinetic of the biodegradability of oxamide-based NPs to achieve safer biomedical nanotools.

Experimental section

Intracellular localization and internalization of BS-FITC NPs

HeLa cells were seeded on glass cover slides, and cultured in EMEM medium containing 10% FBS and 0.1% penicillin-streptomycin at 37°C in a humidified 5% CO₂ atmosphere. After cell attachment, the medium was replaced by fresh medium containing 10 µg/mL of FITC-silica, followed by incubation for 6 h. Cells on cover slides were washed twice with DPBS, then fixed with 4% paraformaldehyde for 1 h and washed 3 times with DPBS. Then, nuclei were stained with DAPI for 3 min and then washed 3 times with DPBS. The cell membrane was stained with CellMask™ deep red plasma membrane dye for 3 min and then washed 3 times with DPBS. Finally, cells were observed with confocal laser scanning microscopy (CLSM, Zeiss LSM 710 upright confocal microscope).

Acknowledgements

The authors gratefully acknowledge King Abdullah University of Science and Technology (KAUST) for the support of this work.

Notes and references

1. J. Croissant, M. Maynadier, A. Gallud, H. Peindy N'Dongo, J. L. Nyalosaso, G. Derrien, C. Charnay, J.-O. Durand, L. Raehm, F. Serein-Spirau, N. Cheminet, T. Jarrosson, O. Mongin, M. Blanchard-Desce,

- M. Gary-Bobo, M. Garcia, J. Lu, F. Tamanoi, D. Tarn, T. M. Guardado-Alvarez and J. I. Zink, *Angew. Chem., Int. Ed.*, 2013, **125**, 14058-14062.
2. J. Croissant, A. Chaix, O. Mongin, M. Wang, S. Clément, L. Raehm, J.-O. Durand, V. Hugues, M. Blanchard-Desce, M. Maynadier, A. Gallud, M. Gary-Bobo, M. Garcia, J. Lu, F. Tamanoi, D. P. Ferris, D. Tarn and J. I. Zink, *Small*, 2014, **10**, 1752-1755.
3. L. Ma, M. Kohli and A. Smith, *ACS Nano*, 2013, **7**, 9518-9525.
4. S. Mura, J. Nicolas and P. Couvreur, *Nature Mater.*, 2013, **12**, 991-1003.
5. J. Croissant and J. I. Zink, *J. Am. Chem. Soc.*, 2012, **134**, 7628-7631.
6. C. Alvarez-Lorenzo and A. Concheiro, *Chem. Commun.*, 2014, **50**, 7743-7765.
7. K. Shao, S. Singha, X. Clemente-Casares, S. Tsai, Y. Yang and P. Santamaria, *ACS Nano*, 2014, **9**, 16-30.
8. B. Moosa, K. Fhayli, S. Li, K. Julfakyan, A. Ezzeddine and N. M. Khashab, *J. Nanosci. Nanotechnol.*, 2014, **14**, 332-343.
9. K. K. Coti, M. E. Belowich, M. Liong, M. W. Ambrogio, Y. A. Lau, H. A. Khatib, J. I. Zink, N. M. Khashab and J. F. Stoddart, *Nanoscale*, 2009, **1**, 16-39.
10. S. Li, B. A. Moosa, J. G. Croissant and N. M. Khashab, *Angew. Chem., Int. Ed.*, 2015, **127**, 6908-6912.
11. J. G. Croissant, O. Mongin, V. Hugues, M. Blanchard-Desce, X. Cattoën, M. Wong Chi Man, M. Maynadier, M. Garcia, M. Gary-Bobo, L. Raehm and J.-O. Durand, *J. Mater. Chem. B*, 2015.
12. M. Wu, Q. Meng, Y. Chen, Y. Du, L. Zhang, Y. Li, L. Zhang and J. Shi, *Adv. Mater.*, 2015, **27**, 189-189.
13. Y. Chen, Q. Meng, M. Wu, S. Wang, P. Xu, H. Chen, Y. Li, L. Zhang, L. Wang and J. Shi, *J. Am. Chem. Soc.*, 2014, **136**, 16326-16334.
14. Q. He, Z. Zhang, F. Gao, Y. Li and J. Shi, *Small*, 2011, **7**, 271-280.
15. J. Croissant, D. Salles, M. Maynadier, O. Mongin, V. Hugues, M. Blanchard-Desce, X. Cattoën, M. Wong Chi Man, A. Gallud, M. Garcia, M. Gary-Bobo, L. Raehm and J.-O. Durand, *Chem. Mater.*, 2014, **26**, 7214-7220.
16. V. P. Chauhan and R. K. Jain, *Nature Mater.*, 2013, **12**, 958-962.
17. A. C. Fonseca, M. H. Gil and P. N. Simões, *Prog. Polym. Sci.*, 2013, DOI: 10.1016/j.progpolymsci.2013.11.007.
18. A. Kumari, S. K. Yadav and S. C. Yadav, *Colloids and Surfaces B: Biointerfaces*, 2010, **75**, 1-18.
19. J. Panyam and V. Labhasetwar, *Adv. Drug Delivery Rev.*, 2003, **55**, 329-347.
20. K. S. Soppimath, T. M. Aminabhavi, A. R. Kulkarni and W. E. Rudzinski, *J. Controlled Release*, 2001, **70**, 1-20.
21. J. Li, Y.-C. Chen, Y.-C. Tseng, S. Mozumdar and L. Huang, *J. Controlled Release*, 2010, **142**, 416-421.
22. G. Bhakta, S. Mitra and A. Maitra, *Biomaterials*, 2005, **26**, 2157-2163.
23. J.-H. Park, L. Gu, G. von Maltzahn, E. Ruoslahti, S. N. Bhatia and M. J. Sailor, *Nature Mater.*, 2009, **8**, 331-336.
24. J. Croissant, X. Cattoën, M. Wong Chi Man, A. Gallud, L. Raehm, M. Maynadier and J.-O. Durand, *Adv. Mater.*, 2014, **26**, 6174-6180.
25. J. Lu, M. Liong, Z. Li, J. I. Zink and F. Tamanoi, *Small*, 2010, **6**, 1794-1805.
26. E. Fleige, M. A. Quadir and R. Haag, *Adv. Drug Delivery Rev.*, 2012, **64**, 866-884.
27. R. Tomlinson, J. Heller, S. Brocchini and R. Duncan, *Bioconjugate Chem.*, 2003, **14**, 1096-1106.
28. E. Cabane, V. Malinova, S. Menon, C. G. Palivan and W. Meier, *Soft Matter*, 2011, **7**, 9167-9176.
29. J. Croissant, M. Maynadier, O. Mongin, V. Hugues, M. Blanchard-Desce, A. Chaix, X. Cattoën, M. Wong Chi Man, A. Gallud, M. Gary-Bobo, M. Garcia, L. Raehm and J.-O. Durand, *Small*, 2015, **11**, 295-299.
30. L. Fertier, C. Théron, C. Carcel, P. Trens and M. Wong Chi Man, *Chem. Mater.*, 2011, **23**, 2100-2106.

31. J. L. Vivero-Escoto, W. J. Rieter, H. Lau, R. C. Huxford-Phillips and W. Lin, *Small*, 2013, **9**, 3523-3531.
32. J. D. Rocca, R. C. Huxford, E. Comstock-Duggan and W. Lin, *Angew. Chem., Int. Ed.*, 2011, **50**, 10330-10334.
33. L.-C. Hu, Y. Yonamine, S.-H. Lee, W. E. van der Veer and K. J. Shea, *J. Am. Chem. Soc.*, 2012, **134**, 11072-11075.
34. J. D. Rocca, M. E. Werner, S. A. Kramer, R. C. Huxford-Phillips, R. Sukumar, N. D. Cummings, J. L. Vivero-Escoto, A. Z. Wang and W. Lin, *Nanomedicine: NBM*, 2015, **11**, 31-38.
35. L.-C. Hu and K. J. Shea, *Chem. Soc. Rev.*, 2011, **40**, 688-695.
36. J. Della Rocca, R. C. Huxford, E. Comstock-Duggan and W. Lin, *Angew. Chem., Int. Ed.*, 2011, **50**, 10330-10334.
37. A. Corma, U. Díaz, M. Arrica, E. Fernández and Í. Ortega, *Angew. Chem., Int. Ed.*, 2009, **121**, 6365-6368.
38. J. L. Vivero-Escoto, W. J. Rieter, H. Lau, R. C. Huxford-Phillips and W. Lin, *Small*, 2013, **9**, 3523-3531.
39. Y. Luo, P. Yang and J. Lin, *Micropor. Mesopor. Mater.*, 2008, **111**, 194-199.
40. J. Croissant, X. Cattoën, M. Wong Chi Man, P. Dieudonné, C. Charnay, L. Raehm and J.-O. Durand, *Adv. Mater.*, 2015, **27**, 145-149.
41. D. Xu, J. Feng and S. Che, *Dalton Trans.*, 2014, **43**, 3612-3617.
42. S. Dib, M. Boufatit, S. Chelouaou, F. Sadi-Hassaine, J. Croissant, J. Long, L. Raehm, C. Charnay and J. O. Durand, *RSC Adv.*, 2014, **4**, 24838-24841.
43. J. J. Moreau, L. Vellutini, M. Wong Chi Man, C. Bied, P. Dieudonné, J. L. Bantignies and J. L. Sauvajol, *Chem. Eur. J.*, 2005, **11**, 1527-1537.
44. S. C. Nunes, K. Bürglová, J. Hodačová, R. A. Ferreira, L. D. Carlos, P. Almeida, X. Cattoën, M. Wong Chi Man and V. de Zea Bermudez, *Eur. J. Inorg. Chem.*, 2015, **2015**, 1218-1225.
45. A. Chemtob, L. Ni, C. Croutxé-Barghorn and B. Boury, *Chem. Eur. J.*, 2014, **20**, 1790-1806.
46. G. Creff, B. P. Pichon, C. Blanc, D. Maurin, J.-L. Sauvajol, C. Carcel, J. J. E. Moreau, P. Roy, J. R. Bartlett, M. Wong Chi Man and J.-L. Bantignies, *Langmuir*, 2013, **29**, 5581-5588.
47. J. J. Moreau, B. P. Pichon, M. Wong Chi Man, C. Bied, H. Pritzkow, J. L. Bantignies, P. Dieudonné and J. L. Sauvajol, *Angew. Chem., Int. Ed.*, 2004, **43**, 203-206.
48. R. Pleixats and M. W. C. Man, *Chem. Asian J*, 2013, **8**, 2235-2241.
49. L. Decker, *New Jersey*, 1977, 27.
50. I. Slowing, B. G. Trewyn and V. S. Y. Lin, *J. Am. Chem. Soc.*, 2006, **128**, 14792-14793.
51. T.-H. Chung, S.-H. Wu, M. Yao, C.-W. Lu, Y.-S. Lin, Y. Hung, C.-Y. Mou, Y.-C. Chen and D.-M. Huang, *Biomaterials*, 2007, **28**, 2959-2966.